Turbulence Regimes and Turbulence Intermittency in the Stable Boundary Layer during CASES-99

JIELUN SUN

National Center for Atmospheric Research, Boulder, Colorado

LARRY MAHRT

Oregon State University, Corvallis, Oregon

ROBERT M. BANTA AND YELENA L. PICHUGINA

NOAA/Earth System Research Laboratory, Boulder, Colorado

(Manuscript received 15 March 2011, in final form 26 July 2011)

ABSTRACT

An investigation of nocturnal intermittent turbulence during the Cooperative Atmosphere–Surface Exchange Study in 1999 (CASES-99) revealed three turbulence regimes at each observation height: 1) regime 1, a weak turbulence regime when the wind speed is less than a threshold value; 2) regime 2, a strong turbulence regime when the wind speed exceeds the threshold value; and 3) regime 3, a moderate turbulence regime when top-down turbulence sporadically bursts into the otherwise weak turbulence regime. For regime 1, the strength of small turbulence eddies is correlated with local shear and weakly related to local stratification. For regime 2, the turbulence strength increases systematically with wind speed as a result of turbulence generation by the bulk shear, which scales with the observation height. The threshold wind speed marks the transition above which the boundary layer approaches near-neutral conditions, where the turbulent mixing substantially reduces the stratification and temperature fluctuations. The preference of the turbulence regimes during CASES-99 is closely related to the existence and the strength of low-level jets. Because of the different roles of the bulk and local shear with regard to turbulence generation under different wind conditions, the relationship between turbulence strength and the local gradient Richardson number varies for the different turbulence regimes. Turbulence intermittency at any observation height was categorized in three ways: turbulence magnitude oscillations between regimes 1 and 2 as wind speed varies back and forth across its threshold value, episodic turbulence enhancements within regime 1 as a result of local instability, and downbursts of turbulence in regime 3.

1. Introduction

Causes of turbulence intermittency include wave instabilities (e.g., Blumen et al. 2001; Balsley et al. 2002; Fritts et al. 2003; Newsom and Banta 2003; Sun et al. 2004; Meillier et al. 2008), density currents (e.g., Sun et al. 2002; Darby et al. 2002), and wind gusts (e.g., Acevedo and Fitzjarrald 2003). Shear instability is the primary turbulence generator in stratified boundary layers, which, through large-eddy overturning, can lead to local thermal instability. Reasons for increased shear vary and may include intrusion of gravity waves and formation of density currents and low-level jets (LLJs). Intermittent turbulence is a distinct characteristic of stable boundary layers. We use intermittent turbulence as defined in the *Glossary of Meteorology* (Glickman 2000, p. 410) as ''the property of turbulence within one air mass that occurs at some times and some places and does not occur at intervening times or places.'' We qualify this definition with the observation that turbulence never completely disappears, but it can become extremely weak (Balsley et al. 2003; Mahrt and Vickers 2006; Banta et al. 2007). Specifically, we use the word ''intermittency'' to describe a temporal variation of turbulence strength observed at a fixed location. Various quantifications of turbulence intermittency can be found in the literature (e.g., Howell

Corresponding author address: Jielun Sun, National Center for Atmospheric Research, P.O. Box 3000, Boulder, CO 80307-3000. E-mail: jsun@ucar.edu

DOI: 10.1175/JAS-D-11-082.1

and Sun 1999; Mahrt 1999; Doran 2004; Drue and Heinemann 2007).

Nocturnal turbulence has been categorized into various turbulence regimes. For example, Mahrt et al. (1998) divided turbulence into weakly stable, transition stability, and very stable regimes based on heat fluxes as functions of atmospheric stability. Van de Wiel et al. (2003) divided nocturnal turbulence into the turbulent regime, intermittent regime, and radiative regime. McNider et al. (1995) studied the probability of stability regimes in nocturnal stable boundary layers in a horizontally homogeneous environment. Because of the radiative cooling on the ground, the nocturnal stable stratification naturally suppresses turbulence.

To understand turbulence intermittency in stable boundary layers, this study focuses on general conditions under which turbulence is enhanced in stable boundary layers. Using the extensive observational dataset obtained from the Cooperative Atmosphere–Surface Exchange Study in 1999 (CASES-99) (section 2), we investigate and categorize patterns of turbulence regimes (section 3). We then categorize turbulence intermittency based on the turbulence regimes and demonstrate an example from each turbulence intermittency category (section 4). Section 5 is the summary.

2. Observations

The CASES-99 field experiment (Poulos et al. 2002; Sun et al. 2002) includes three-dimensional turbulence observations at nine levels (eight levels at a given time) on a 60-m tower over relatively flat terrain. Sonic anemometer turbulence measurement levels were at 1.5, 5, 10, 20, 30, 40, 50, and 55 m. The lowest sonic anemometer was moved from 1.5 to 0.5 m on 20 October. Together with the slow-response wind vanes at four levels (15, 25, 35, and 45 m), a total of 12 levels of wind observation on the 60-m tower were used in this study. The slow-response wind observations were calibrated to the sonic anemometer measurements for the accuracy of the sonic anemometer.

Thermocouple temperature measurements at 34 levels (0.23, 0.67, 2.3 m, and every 1.8 m above 2.3 m) were recorded with three dataloggers (Burns and Sun 2000). One measurement from each datalogger was placed at one level for side-by-side comparison. The thermocouple temperature at 55 m was calibrated against the mechanically aspirated temperature at 55 m, and the difference between the two temperature measurements at 55 m was used to calibrate the absolute thermocouple temperature at the rest of the levels. Atmospheric pressure was measured at three levels on the 60-m tower: 1.5, 30, and 50 m. Pressure decreased approximately linearly with height because of the relatively thin tower layer compared to the scale height of atmospheric pressure. We used the pressure measurements on the 60-m tower to calculate the potential temperature and to convert relative humidity to specific humidity.

High-resolution Doppler lidar (HRDL), a scanning, coherent Doppler lidar system designed for atmospheric boundary layer research (Grund et al. 2001; Pichugina et al. 2008), was located 1.45 km southeast of the 60-m tower. Its range resolution, minimum range, and maximum range during CASES-99 were 30 m, 250 m, and 2–6 km, respectively.

In addition to the above directly observed variables, some calculated variables were used in this study. Turbulent fluxes based on 10-min data segments were calculated after removing mesoscale fluctuations, such as gravity waves, based on the method of Vickers and Mahrt (2003, 2006). Because the calculated turbulent fluxes closely agree with the 5-min unweighted fluxes, 5-min data segments were used to calculate standard deviations of all the variables, vertical shear, and vertical temperature gradients at all the sonic anemometer observation levels. For investigation of the relationship between turbulent fluxes and other variables only, the variables at 5-min intervals were averaged to 10-min intervals to match the flux dataset. The method for calculating local wind shear was described in Sun (2011). Briefly, the local shear at each observation level was calculated analytically from the wind profile that was locally fitted to a log-linear profile using observed winds, one level above, and one level below. The accurate high-vertical resolution ($\leq$1.8 m) thermocouple temperature and the simple linear finite differencing method were used to calculate vertical temperature gradients. The calculated local shear $\partial\overline{\mathbf{V}}/\partial z$ (where $\mathbf{V}$ and z are the horizontal wind speed vector and the height above the ground, and the overbar represents time averaging) and the vertical temperature gradient $\partial\overline{\theta}/\partial z$ (where θ is the potential temperature) were used to calculate the local gradient Richardson number $\mathrm{Ri} \equiv (g/T_0)\partial\overline{\theta}/\partial z(\partial\overline{\mathbf{V}}/\partial z)^{-2}$ (g and T_0 are the gravity constant and a reference temperature, respectively).

Since the sonic anemometers were all mounted on booms pointing eastward, turbulent fluxes associated with winds from 270° $\pm$ 60° could be distorted by the 60-m tower; therefore, all the flux data from this sector were eliminated from this analysis. All the nighttime data obtained from 1800 to 0600 LST, 5–29 October except those subject to the flow distortion were used in this study. The dates in this study are labeled based on UTC. For example, the night of 25 October and the early morning of 26 October is from 0000 to 1200 UTC 26 October; therefore, we labeled this night as 26 October.

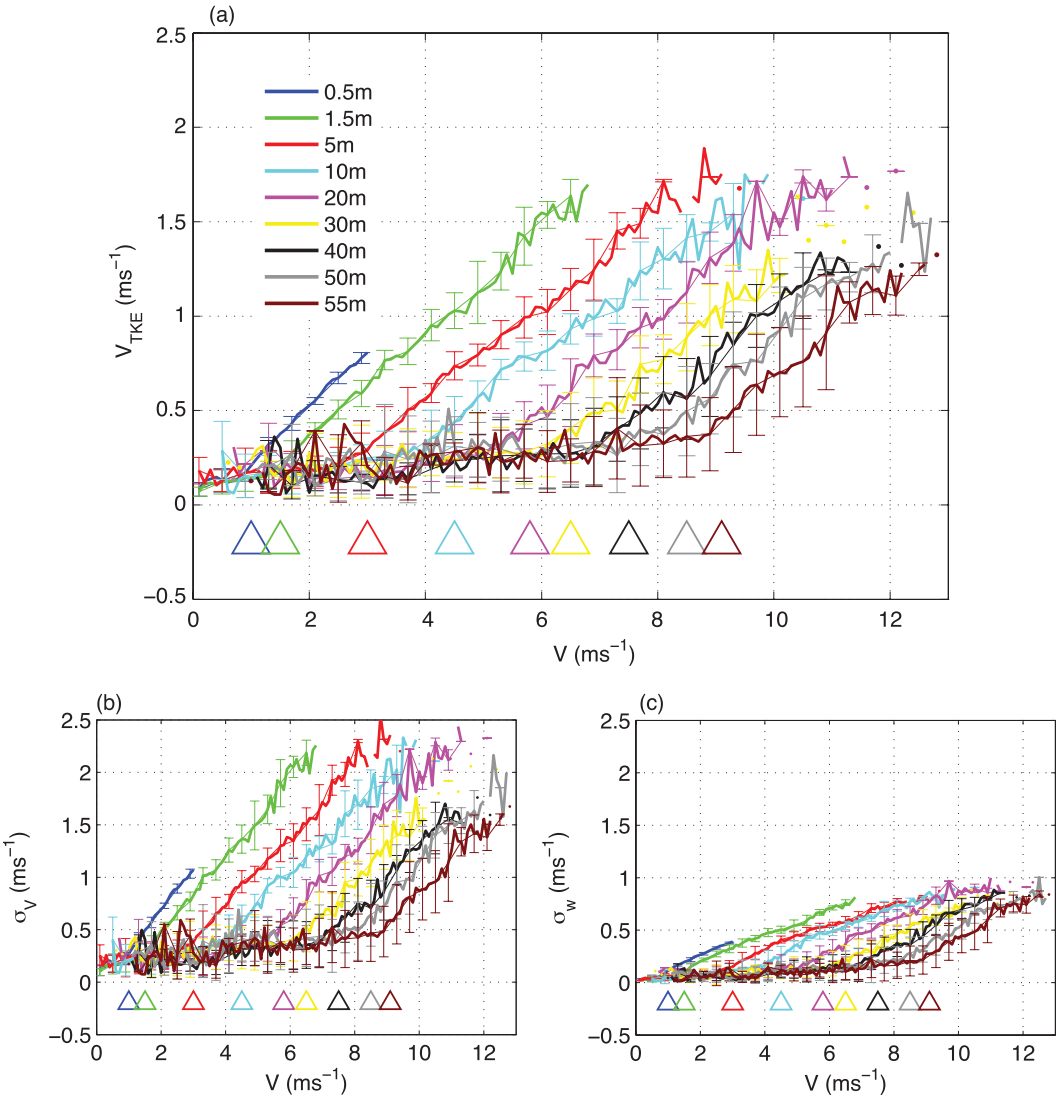

FIG. 1. The relationship (a) between the bin-averaged turbulence strength V_{TKE} and the wind speed V, (b) between the bin-averaged standard deviation of the wind speed σ_V and V, and (c) between the bin-averaged standard deviation of the vertical velocity σ_w and V at the nine observation levels. In each panel, the standard deviation of the variable in ordinate within each V bin is marked by a vertical line. The threshold wind speed at each level is marked with a triangle in the color of the height. The data are from the entire CASES-99 dataset as described in the text.

3. Turbulence regimes

In this section, we explore the dependence of turbulence on mean wind speed, local shear, local thermal stratification, and Ri to identify possible turbulence regimes.

a. Dependence of turbulence on shear instability

We use the turbulence velocity scale defined as $V_{\mathrm{TKE}} = [(1/2)(\sigma_u^2 + \sigma_v^2 + \sigma_w^2)]^{1/2} = \sqrt{\mathrm{TKE}}$ to represent turbulence strength, where TKE represents the turbulent kinetic energy, u, v, and w are the zonal, meridional, and vertical wind components, and σ represents the standard deviation of each variable. The relationship between V_{TKE} and mean horizontal wind speed, $V = |\mathbf{V}|$, at each observation level is shown in Fig. 1a. The relationship is similar between levels, consisting of a regime where V_{TKE} is weak and increases only slightly with V (regime 1) and a regime where V_{TKE} increases rapidly with V after V exceeds a threshold value (regime 2) (Fig. 2). The threshold value increases with height approximately logarithmically (Fig. 3a), resulting in a shift of the regime-2 curves in Fig. 1a to the larger wind speed values as the measurement height increases. Similarly, the standard deviations of the horizontal wind speed σ_V and of the

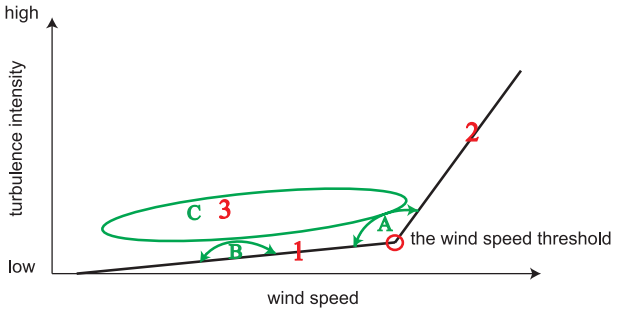

FIG. 2. Schematic of the three turbulence regimes (red numbers) and the three categories of turbulence intermittency (green letters) commonly observed during CASES-99 at each observation height. Turbulence in regime 1 is mainly generated by local instability. Turbulence in regime 2 is mainly generated by the bulk shear. Turbulence in regime 3 is mainly generated by top-down turbulent events.

vertical velocity σ_w are also related to V (Figs. 1b,c), except the slope of σ_w versus V increases with height because of the ground impingement on turbulent eddies (Sun 2011). As the wind speed approaches zero, σ_w approaches zero, but not σ_V, indicating that σ_V includes relatively large nonturbulent eddies. Although one may be tempted to associate the threshold wind speed with a critical or transitional Richardson number, the results below do not support such a concept.

In regime 2, V_{TKE} increases strongly and linearly with V at a slope of ~0.25 at all the observation levels when the wind speed exceeds its threshold value (Fig. 3b). The relatively constant slope is due to the dominant relationship between σ_V and V as shown in Fig. 1b. Regime 2 occurs when turbulence approaches near neutral, which is demonstrated in the sharp increase of the local Obukhov length Λ (Fig. 3d). The local Obukhov length here is defined as $\Lambda \equiv \overline{\theta} u_*^2/\kappa g \theta_*$, where u_* is related to the local momentum flux τ as $u_* = \sqrt{\tau/\rho}$ (where ρ is the air density); $\theta_* \equiv -\overline{w'\theta'}/u_*$; $\overline{w'\theta'}$ represents heat fluxes; and κ is the von Kármán constant. The approximation $\theta_v \simeq \theta$ is relatively accurate for the present dataset. Because turbulence is mainly generated by shear instability at night when the buoyancy flux is negative, the close relationship between V and V_{TKE} for regime 2 suggests that near the ground, turbulence under stronger winds responds to the bulk shear defined here as the mean wind divided by its

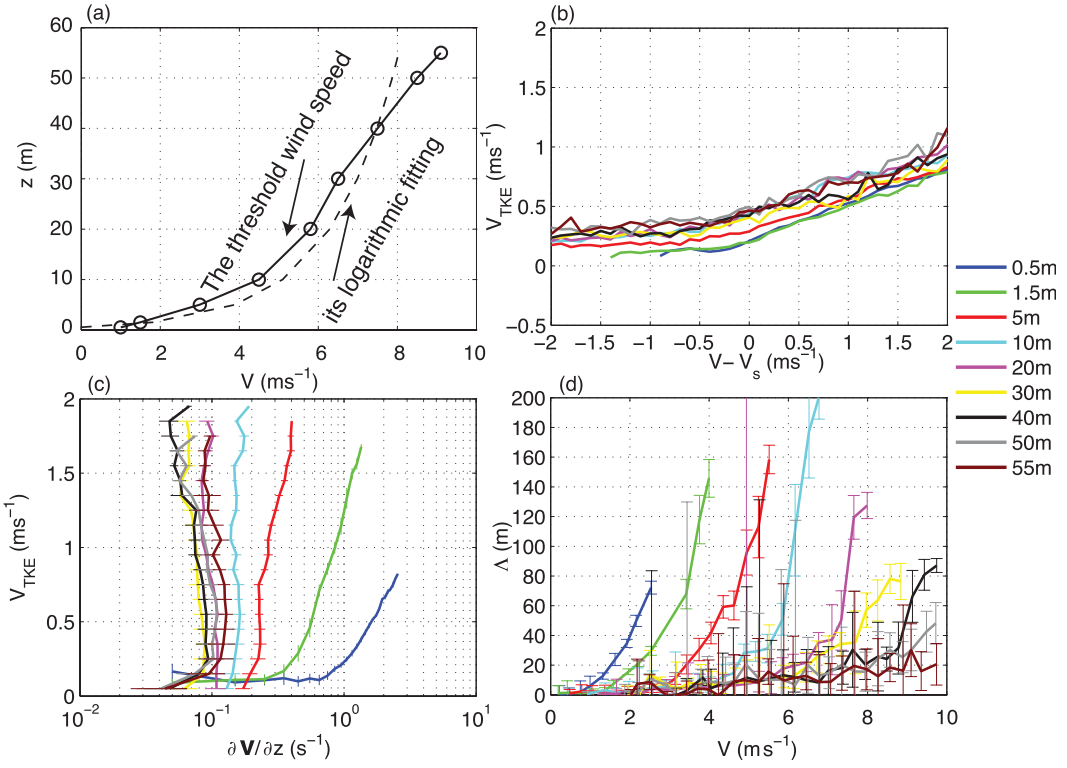

FIG. 3. (a) The threshold wind speed as a function of height (solid line with circles) and its logarithmic fitting (dashed line); (b) V_{TKE} as a function of the wind speed V relative to its threshold value V_s at the nine observation levels. Also shown is the relationship (c) between V_{TKE} and local shear and (d) between V_{TKE} and the local Obukhov length Λ at the nine observation levels. The standard deviation of V_{TKE} at each local shear bin at $z = 0.5$ and 1.5 m and the standard deviation of the local shear at each V_{TKE} bin for z above 1.5 m are plotted in (c); and the standard deviation of Λ within each V bin is plotted in (d).

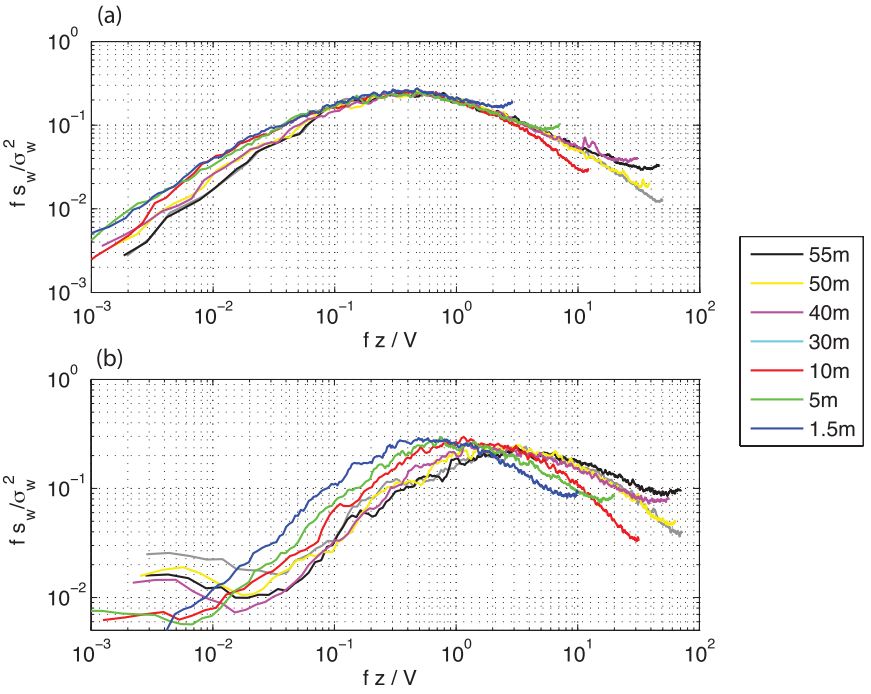

FIG. 4. The power spectra of the vertical velocity s_w normalized by the w variance σ_w^2 as a function of the frequency f normalized by the inverse of the bulk shear for (a) the wind speed above the threshold value during the night of 17 October, and (b) the wind speed less than the threshold value during the night of 5 October. A 4-h data segment is used at each observation height in both panels.

observation height (i.e., V/z). Spectral analyses of w indeed indicate that when V exceeds the threshold value, the w power spectra have well-defined peaks at the frequency V/z at all the levels (Fig. 4a). This result implies that the kinetic energy of turbulent eddies is generated at the frequency associated with the bulk shear and that the energetic turbulence eddies scale with height when wind speed exceeds its threshold. Because the strong wind speed tends to increase linearly with height away from the ground due to turbulent mixing (section 3d), the local shear, which was calculated using the wind observations within a vertical layer of less than 10 m, tends to cluster around 0.1 s^{-1} as also noted by Banta et al. (2003, 2006). Consequently, strong turbulence becomes independent of the local shear as demonstrated in Fig. 3c except close to the ground, where the local and bulk shears are closely related to each other.

In contrast to regime 2, the local shear is responsible for generating small eddies and weak turbulence in regime 1, which is illustrated by the close relationship between V_{TKE} and local shear for weak turbulence (Fig. 3c). In this situation, the w power spectra peak at wavelengths smaller than their observation heights (Fig. 4b), which indicates that the local shear-generated eddies are too small to interact with the ground directly. This situation is sometimes called the decoupled boundary layer (e.g., Acevedo and Fitzjarrald 2003; Mahrt and Vickers 2006). Any implication of the roles of local and bulk shear in similarity theory is outside of the scope of this study and will be investigated in a separate paper.

The observation of the turbulence spectral peak scaling with wind speed and observation height was also found by Panofsky and McCormick (1960). The role of the bulk shear in turbulence generation was also implicitly illustrated in the close relationship between turbulence and the bulk Richardson number in Mahrt (2008), where the bulk Richardson number was defined based on the wind and temperature observations between the observation height and the 1-m level.

b. *Dependence of turbulence on local stratification and local instability*

Vertical temperature gradients are generally positive at night and theoretically limit turbulence growth. We found that V_{TKE} is weakly dependent on local $\partial\overline{\theta}/\partial z$ in regime 1 when the wind speed is less than the threshold value (blue dots in Fig. 5). As V increases above its threshold value, V_{TKE} in regime 2 decreases sharply with increasing $\partial\overline{\theta}/\partial z$ (red dots in Fig. 5). In other words, even though the stratification is often weaker for winds above

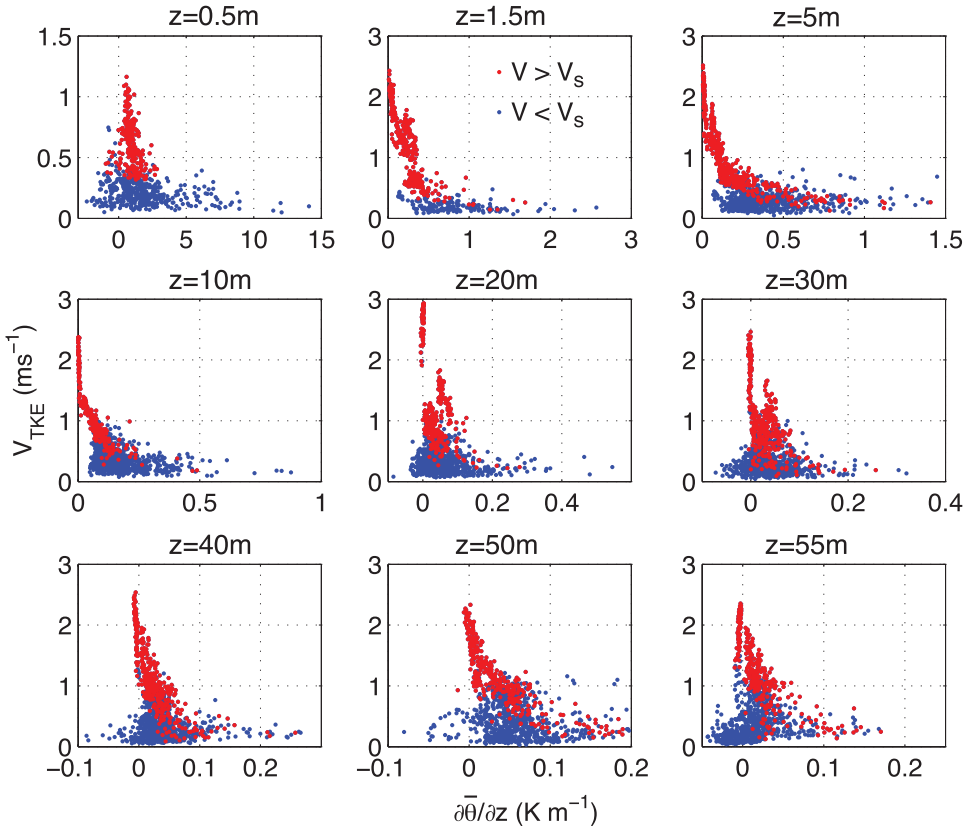

FIG. 5. The relationship between the local vertical gradient of potential temperature $\partial\overline{\theta}/\partial z$ and V_{TKE} at the nine sonic anemometer levels. The red and blue colors are for wind speed larger than and smaller than the threshold value V_s, respectively, and each dot is from a 5-min data segment.

the threshold value compared to winds below its threshold value, the turbulence seems more closely related to the stratification in regime 2 than that in regime 1.

As θ_* is directly related to the sensible heat flux, we examined the relationship between V and θ_*. We found that θ_* is approximately linearly correlated with temperature fluctuations, σ_θ, at each level (Fig. 6a), and θ_* reaches a maximum when the wind speed reaches its threshold value (Fig. 6b). The increase of θ_* with V before V reaches its threshold indicates that the increasing turbulence enhances temperature fluctuations as the source of the temperature fluctuation is provided by the vertical temperature gradient, which is constantly reinforced by the radiative cooling, especially under weak winds. As the wind speed increases above the threshold value, the decrease of θ_* with V is associated with decreased vertical temperature gradient resulting from stronger mixing by the large eddies generated by the bulk shear. Vanishing stratification leads to vanishing temperature fluctuations and heat fluxes. The contrast between the general monotonic increase of V_{TKE} with V and the increase and decrease of θ_* with V before and after the wind threshold suggests that the steep negative correlation between V_{TKE} and $\partial\overline{\theta}/\partial z$ for V greater than its threshold value is a result of the strong turbulent mixing, not the suppression of turbulence by the stratification. On average, the change of the wind speed is much faster than the establishment of the stratification. Because of the dominant role of the turbulent mixing in generating heat flux under stable conditions, both σ_V and σ_w are similarly related to V (Fig. 1) even though σ_w, but not σ_V, is strongly related to the heat flux.

The increase and decrease of θ_* with V was presented in terms of the sensible heat flux change in Mahrt et al. (1998) to distinguish the weakly stable from the moderately stable turbulent regimes. Similar relationship between θ_* and u_* was also found by Holtslag and De Bruin (1988).

Normally the local gradient Ri would be considered as more universal than wind speed in the prediction of turbulence generation as it combines the effects of both local shear and buoyancy. However, if the bulk shear, not local shear, is responsible for turbulence generation, the local Ri does not capture the turbulence generation mechanism. When the wind speed is below its threshold value and turbulence is controlled by local shear, V_{TKE}

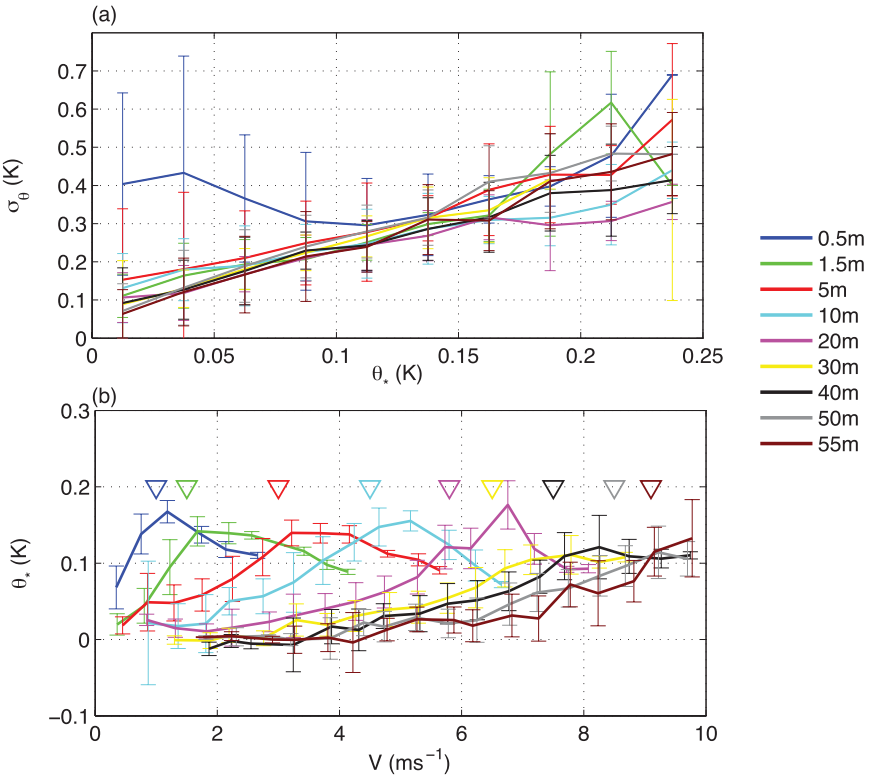

FIG. 6. The composite relationship (a) between θ_* and the standard deviation of the potential temperature σ_θ, and (b) between the wind speed V and θ_*. The threshold wind speed at each level is marked with a triangle in the color of the height in (b). Note that θ_* reaches its maximum value approximately at its threshold wind speed in (b).

decreases gradually with increasing Ri even though $\partial\overline{\theta}/\partial z$ is only weakly related to V_{TKE}. When the wind speed is above its threshold value, turbulence generated by the bulk shear results in a sharp decrease of $\partial\overline{\theta}/\partial z$, leading to the apparent sensitivity of V_{TKE} to $\partial\overline{\theta}/\partial z$, thus the apparent dependence of V_{TKE} on Ri (e.g., the red dots in Fig. 7) even though local shear does not contribute significantly to the turbulence generation in this situation.

The different V_{TKE}–Ri relationships in regimes 1 and 2 are schematically illustrated in Fig. 8. The range of the V_{TKE} variation is relatively small in regime 1 even though the range of the Ri variation is large. In contrast, the range of the V_{TKE} variation is large while both the variability and the magnitude of Ri are relatively small in regime 2. The transition of the V_{TKE}–Ri relationship between regimes 1 and 2 can be abrupt. Consequently, the Ri value for strong V_{TKE} in regime 2 (point b in Fig. 8) can be larger than the Ri value for much weaker V_{TKE} in regime 1 (point a in Fig. 8). Once the bulk shear starts to play a major role in turbulence generation, Ri is generally smaller than 0.2. Overall, Ri is associated with local gradients that govern small eddies and fails to include the influence of instabilities over deep layers. Therefore, V_{TKE} is better correlated with wind speed than with local Ri in regime 2. As the magnitude of the sensible heat flux is controlled by the strength of the turbulence and the temperature perturbation, the relationship between the sensible heat flux and Ri also varies between regimes 1 and 2. Einaudi and Finnigan (1993) also found poor correlation between Ri and turbulence and attributed it to nonlocal interactions between gravity waves and turbulence. Recent investigation demonstrates that the universal critical Richardson number varies between flows (e.g., Canuto 2002) or may not exist at all (e.g., Galperin et al. 2007; Zilitinkevich et al. 2007; Mahrt 2010b).

c. *Turbulence regimes*

We have identified two turbulence regimes for CASES-99 based on the relationship between wind speed and V_{TKE} (i.e., regimes 1 and 2 in Fig. 2). In addition to these two regimes, moderate turbulence is often generated above the observation level and diffuses downward, such as the case analyzed by Blumen et al. (2001) and Newsom and Banta (2003). They found that turbulence was generated from large eddy overturning as a result of Kelvin–Helmholtz (K–H) instability. As we will show in

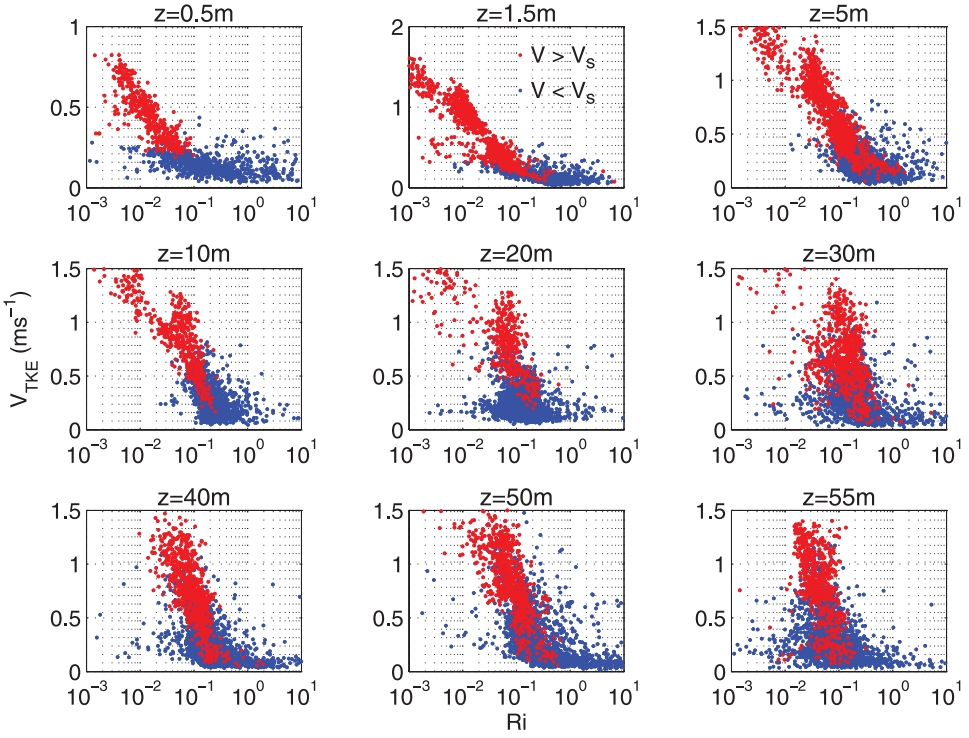

FIG. 7. The relationship between the local gradient Richardson number Ri and V_{TKE} for wind speed larger than (red) and smaller than (blue) its threshold value V_s at the nine sonic anemometer levels. Each dot is calculated using a 5-min data segment.

section 4c, moderate turbulence above the weak "background" turbulence appears at the highest observation level first and spreads gradually to lower levels. As the strength of the top-down turbulent event weakens, the moderate turbulence decays at the lowest level first and gradually at the levels above. As a result, the duration of the occurrence of the moderate turbulence visibly increases with height (section 4c).

To distinguish the turbulence generated by top-down turbulent events from that generated by either the local or the bulk shear, we define the top-down turbulent regime as regime 3 in Fig. 2. The relationship between V_{TKE} and V for some of the top-down turbulent events is shown in Fig. 9. Because local shear-generated turbulence can occur near the ground while the layer aloft can be simultaneously influenced by downward-propagating turbulent events, and the background environment is always turbulent even though the turbulent fluxes can be extremely weak (Mahrt and Vickers 2006), Fig. 9 includes some of background weak turbulence. During the entire CASES-99 field program, the percentage of the time series in regime 3 is small compared to regime 1; therefore, regime 1 is prominent when the wind speed is less than its threshold value (Fig. 1a). Because the data segments used to calculate V_{TKE} may include nonturbulent components, regime 3 occasionally includes nonturbulent wind oscillations when the mean wind is very weak.

d. LLJ and the turbulence regimes

The occurrence of the different regimes is closely related to the LLJ. Without a strong LLJ, the wind over

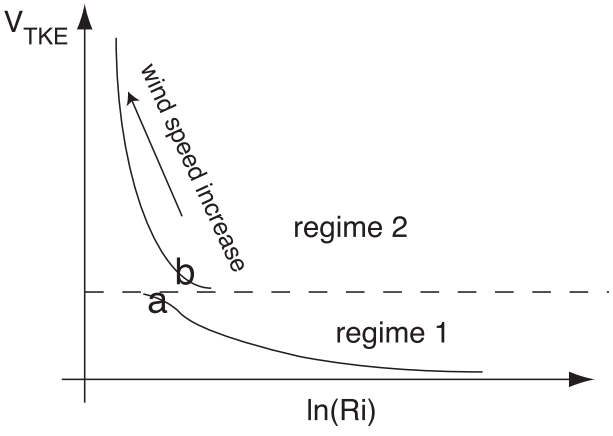

FIG. 8. Schematic summary of the relationship between V_{TKE} and the local Ri at a fixed observation height. The horizontal dashed line separates regime 1 from regime 2. Note that V_{TKE} at a can be smaller than V_{TKE} at b even when Ri at a is smaller than Ri at b.

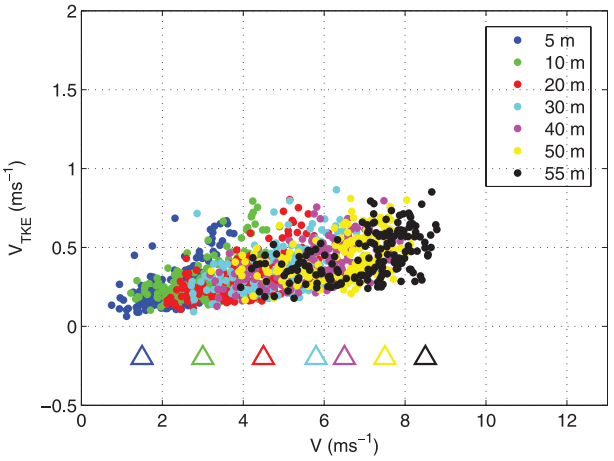

FIG. 9. The relationship between V_{TKE} and wind speed V at seven observation heights during the periods when turbulence was generated from clearly identifiable downward-propagating events. Each dot represents a 5-min data segment. The threshold wind at each level is marked with a triangle in the color of that height.

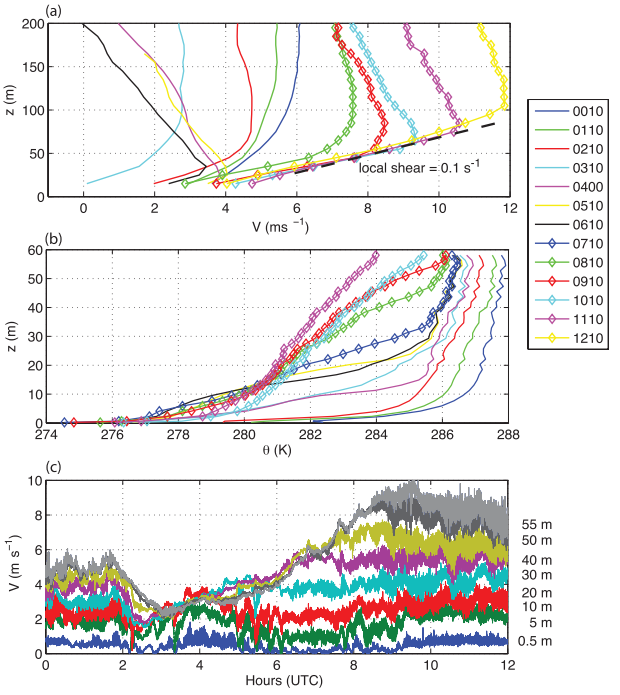

FIG. 10. (a) The lidar wind speed profiles, (b) the potential temperature profiles from the thermocouple measurement on the 60-m tower, and (c) the time series of the wind speed at the eight sonic anemometer levels during the night of 20 October. The relationship among the turbulence strength (which is visible from the wind speed fluctuations), the development of LLJs, and the impacts of the turbulence on the vertical variation of the potential temperature are evident from the three panels. The wind profiles were measured by the HRDL averaged for 10 min at the beginning of each hour. Sunset was at 16 min before 0000 UTC. The dashed black line in (a) marks the local shear of 0.1 s^{-1}.

the entire 60-m tower layer is weak and regime 1 prevails. An example is shown in Fig. 10 before 0900 UTC on the night of 20 October, which is analyzed in detail by Banta et al. (2002, 2007). The strengthening of the LLJ after 0900 UTC increases local shear below the LLJ toward the value of ~0.1 m s^{-1}, which is also demonstrated in Fig. 3c. Because the vertical temperature gradient decreases with height under weak winds (Fig. 10b), with approximately constant local shear, the turbulence increases with height (Fig. 10c). Consequently the top-down turbulent event (i.e., turbulence regime 3) appears.

Another example of the connection between LLJs and the turbulence regimes is in Fig. 11 when LLJs lead to wind speeds above their thresholds. As the LLJ wind speed U_J increases, the LLJ height Z_J also tends to increase (Fig. 11a), which is also shown in our Fig. 10a, as well as in Banta et al. (2002) and Pichugina et al. (2008). Associated with the variation of the LLJ wind speed and height, the standard deviation of the horizontal wind observed by the lidar σ_U below Z_J increases as well (Fig. 11b), as shown by Banta et al. (2006) and Banta (2008). Consequently, σ_U at a constant height Z_1 changes from a small constant value when the wind speed at Z_1 is less than its threshold value to a value increasing with wind speed after the wind speed exceeds its threshold (Fig. 11c). The turbulence at Z_1, therefore, jumps from regime 1 to regime 2 as illustrated in Fig. 2.

4. Categories and examples of turbulence intermittency

Associated with the three turbulence regimes, three categories of turbulence intermittency are observed during CASES-99 (Fig. 2). In category A, when the wind speed oscillates across its threshold value, turbulence is enhanced when the wind speed exceeds its threshold value and is reduced when the speed falls below it (i.e., turbulence changes between regime 1 and regime 2). In category B, when the wind speed resulting from atmospheric disturbances remains less than the threshold value, the disturbances intermittently reduce the local stability and slightly increase the local turbulence (i.e., turbulence episodically enhances within regime 1). In category C, when top-down turbulent events suddenly intrude downward into a weak turbulent environment, turbulence regime 3 occurs.

a. Category A turbulence intermittency

Turbulence intermittency during CASES-99 frequently occurs when the wind speed oscillates between regimes 1 and 2 (i.e., category A turbulence intermittency). In general, nonturbulent wind oscillations can be caused by various physical mechanisms, including internal gravity

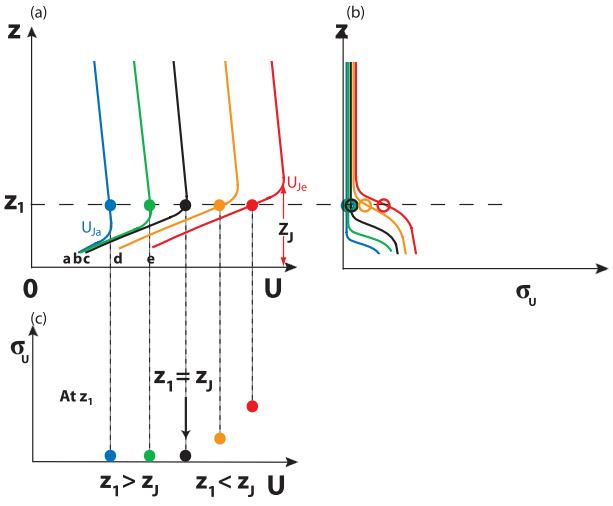

FIG. 11. A schematic summary of the vertical variation of (a) the streamwise wind speed U of a LLJ and (b) its standard deviation σ_U from a to e, which in general would be from different nights, and (c) the relationship between U and σ_U at height Z_1 from *a* to *e* based on the CASES-99 nighttime lidar data. In (a), U_{Ja} and U_{Je} represent the maximum wind of the LLJ at a and e, respectively; Z_J represents the height of the lowest wind maximum of an LLJ as defined in Banta et al. (2002).

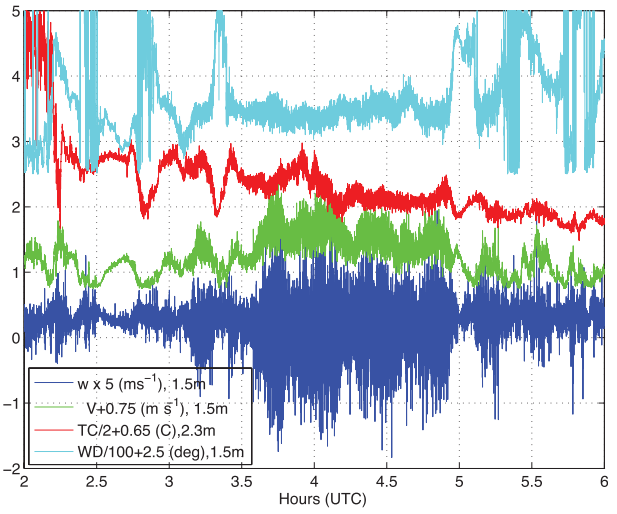

FIG. 12. The intermittent turbulence resulting from nonturbulent wind speed oscillations during the night of 20 October. The plot shows the time series of the wind speed V, the vertical velocity w, and the wind direction (WD) at 1.5 m above ground, and the thermocouple temperature (TC) at 2.3 m. All the variables are scaled as indicated in the figure legend for easy comparison. All the turbulence enhancements are associated with wind speed increases.

and solitary waves. These wave events are sometimes related to density currents (e.g., Sun et al. 2002) and other mesoscale disturbances (e.g., Acevedo and Fitzjarrald 2003). Here we demonstrate an example of this type of turbulence intermittency on the night of 20 October (Fig. 12), which was analyzed by Banta et al. (2007). Around 0230 UTC, wind speed oscillations are small and do not lead to wind speed above the threshold value at any level. The weak turbulence allows strong large-scale temperature and vertical velocity oscillations and wind direction rotation with height in the direction consistent with the Ekman spiral discussed by Grachev et al. (2005). When the amplitude of the wind oscillation increases, turbulence is enhanced whenever the wind speed exceeds its threshold value at 1.5 m, which is evident in the time series of wind speed and vertical velocity in Fig. 12. The strong turbulent mixing between 0330 (3.5) and 0500 UTC reduces the vertical temperature gradient and the wind direction difference with height and therefore reduces temperature and wind direction oscillations.

b. *Category B turbulence intermittency*

An example of category B turbulence intermittency, which is also examined by Banta et al. (2007), occurs at 30 and 50 m after 0206 (2.1) UTC 26 October (Fig. 13). In this case, relatively weak turbulence is generated by local shear in a steady stratified environment. This enhanced turbulence is still sufficiently weak that turbulence at the adjacent levels is not detectably affected. The enhancement of local shear can also be caused by atmospheric waves having relatively small wind speed amplitude such that the composite wind speed is less than its threshold value, and the turbulence change is within regime 1 (not shown). Mahrt (2010a) found that with very weak winds and strong stratification, the turbulence appears to respond mainly to waves and other small-scale nonturbulent motions.

c. *Category C turbulence intermittency*

An example of category C turbulence intermittency is the top-down turbulent events in Fig. 14. During this night, moderate turbulent events occur when the wind is weak as shown by red dots in Fig. 14c. The top-down events are evident in the increasing duration and strength of turbulence with height, such as the event just before 0600 UTC (Fig. 15a). Commonly the top-down turbulent event is associated with K–H instability as demonstrated in Blumen et al. (2001). As a result of large-eddy overturning associated with such instabilities, negative temperature gradients are often observed and the total number of the small-negative-temperature-gradient occurrences increases with height as the turbulence spreads toward the ground as shown in Fig. 14a. Occurrences of small negative vertical temperature gradient statistically increase with height, which is visible in Fig. 5. As a result of episodic intrusions of the top-down turbulent events into the otherwise regime-1 turbulent environment, category C turbulence intermittency occurs (Fig. 15a). Nonturbulent wind oscillations under weak mean winds

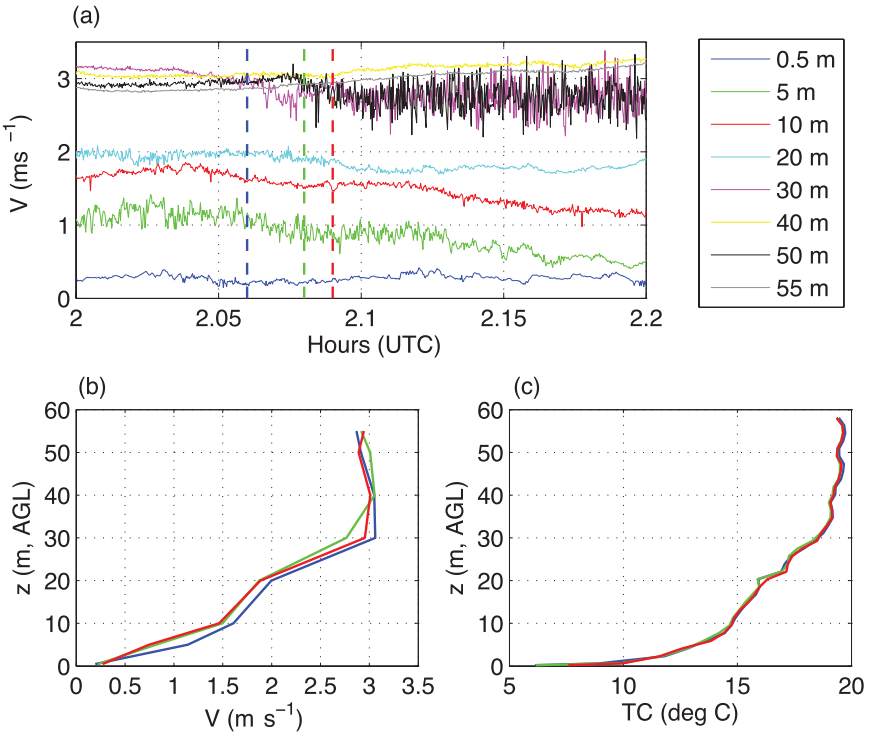

FIG. 13. The turbulence in response to the local shear increase on 26 October, a night having very stable boundary structure according to Banta et al. (2007). The wind speed V and thermocouple temperature (TC) profiles in (b) and (c) are observed at the times marked in (a) with the dashed lines in the same colors.

can also inadvertently lead to large computed V_{TKE} values as shown in Fig. 15b.

5. Summary

By analyzing the entire nocturnal CASES-99 dataset, we identified three turbulence regimes depending on how turbulence was generated. Regime 1 is the weak turbulence regime when the wind speed is less than its threshold value. Turbulence in this regime is generated by local shear instability and modulated by vertical temperature gradients. The length scale of the local shear is smaller than the observation height; therefore, eddies generated by the local shear do not directly interact with the ground. Regime 2 is the strong turbulence regime when the wind speed exceeds its threshold value, and the turbulence increases systematically with increasing wind speed. In this regime, the turbulence is generated by the bulk shear defined as the mean wind divided by the observation height. Regime 3 is the turbulence regime when the wind speed is below its threshold value and top-down turbulence sporadically bursts into the otherwise weak turbulence regime. Occasionally regime 3 includes nonturbulent wind oscillations when the mean wind speed is weak. The composite threshold wind speed increases approximately logarithmically with height, which marks the transition of turbulence generation by local shear to bulk shear. This transition cannot be described by the local or bulk Richardson number alone.

The local gradient Richardson number by definition is associated with local shear and local stratification; therefore, it only captures the turbulence generation mechanism when wind speed is below the threshold value. Once the bulk shear enhances the TKE on scales associated with the observation height, the increased turbulent mixing decreases the local vertical temperature gradient. The reduction of the vertical temperature gradient leads to decreasing temperature perturbations and θ_* with wind speed. Consequently the threshold wind speed also represents the wind speed at which θ_* reaches its maximum value. The reduced local vertical temperature gradient occurring after the wind speed exceeds its threshold value leads to the sharp reduction of the local gradient Richardson number even though the turbulence is not related to the local shear when the wind speed exceeds the threshold value. In contrast to regime 2, the turbulence strength in regime 1 increases gradually with decreasing local gradient Richardson number, and the relationship is not as tightly catenated as the one in regime 2. The significantly different relationship between

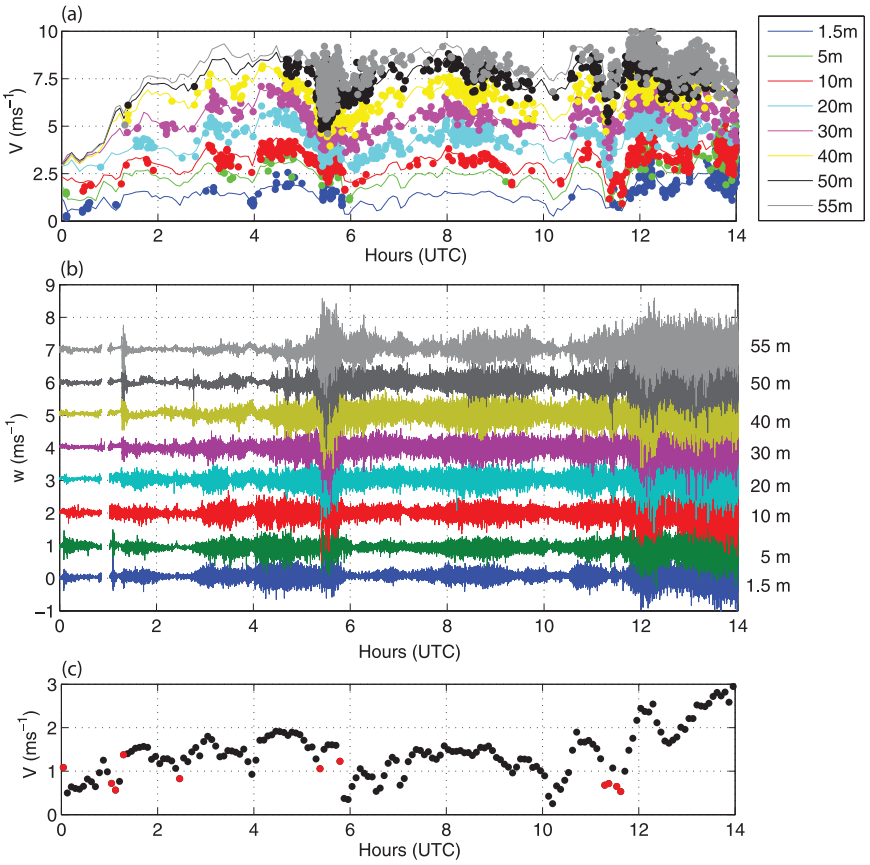

FIG. 14. The time series of (a) the wind speed from the eight sonic anemometers (colored solid lines) with the negative vertical temperature gradient at each level marked in the color of that height, (b) the vertical velocity at the eight levels, and (c) the wind speed at 1.5 m for the night of 6 October. The occurrences of moderate turbulence under weak winds are marked in red in (c). In (b), the zero vertical velocity at the observation height above 1.5 m is incremented by 1 m s^{-1} from the level below for visibility. Each dot in both (a) and (c) represents a 5-min data segment.

turbulence and Ri in regime 1 and 2 cannot be described by a single formulation since the local gradient Richardson number associated with a strong turbulence case in regime 2 can be larger than the one for a weak turbulence case in regime 1. A similar discontinuity at the threshold wind speed also occurs in the relationship between sensible heat fluxes and Ri.

The three turbulence regimes are closely related to nocturnal LLJs. Without a strong LLJ, the wind shear and turbulence over the entire boundary layer below the LLJ are weak. As a result, turbulence regime 1 prevails. When the maximum wind of a LLJ is less than the threshold value for its height above the ground, but the local shear below the LLJ is significant, moderate turbulence can be generated by local shear instability and diffuse downward, especially when the vertical temperature gradient decreases with height. This situation corresponds to the turbulence regime 3, which may be imposed on the background environment with regime-1 turbulence. If the LLJ is strong enough to increase the wind speed above its threshold value, regime 2 occurs. Both regimes 2 and 3 are commonly associated with LLJs or mesoscale wind events.

Turbulence intermittency is generated by episodic generation of turbulence in the generally weak-wind nocturnal boundary layer. Three categories of turbulent intermittency during CASES-99 are associated with turbulence variations between the three turbulence regimes. Turbulence intermittency may occur when the wind oscillates across its threshold value (i.e., turbulence oscillates between regimes 1 and 2, which is category A turbulence intermittency). The turbulence intermittency may also occur when local turbulence is enhanced by local instability (i.e., turbulence variation within regime 1, which is category B turbulence intermittency). The turbulence intermittency may also appear when top-down

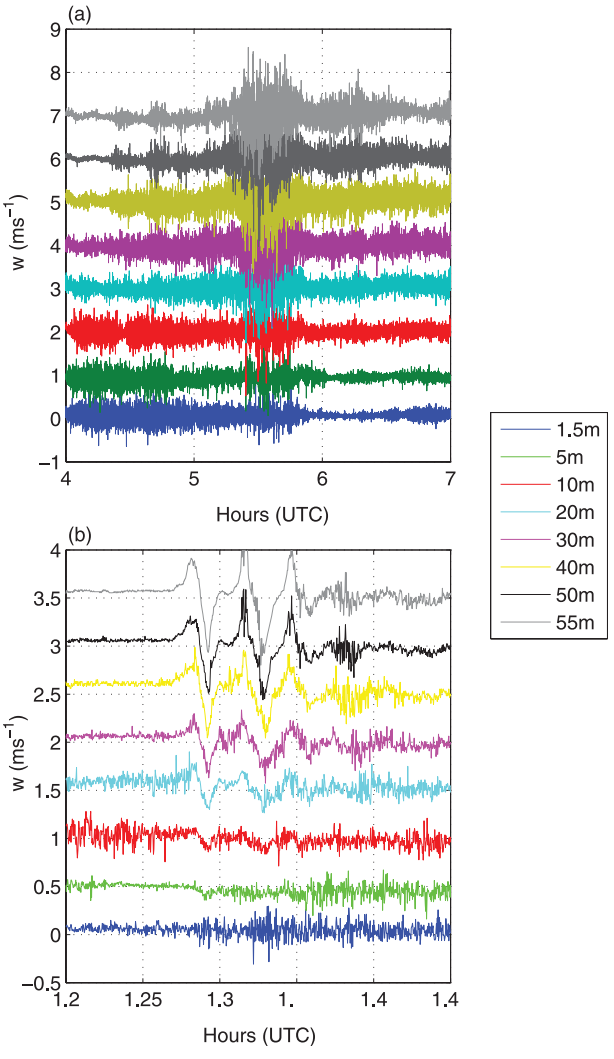

FIG. 15. The time series of the vertical velocity w from the eight sonic anemometers for two time periods during the night of 6 October. The zero vertical velocity at the observation height above 1.5 m is incremented by (a) 1 and (b) 0.5 m s^{-1} from the level below for visibility.

turbulent events diffuse downward into a weak-turbulence environment (i.e., the occurrence of regime 3, which is category C turbulence intermittency).

Acknowledgments. The authors would like to acknowledge the field support from the Earth Observing Laboratory of the National Center for Atmospheric Research and the graphic help from Lisa Darby. The authors would also like to thank Otávio Acevedo and the other two anonymous reviewers for their constructive and valuable comments.

The study was supported by U.S. Army Research Office, MIPR3KNSFAR057, and the NOAA Air Quality Program. The University Corporation for Atmospheric Research manages the National Center for Atmospheric Research under sponsorship by the National Science Foundation. Any opinions, findings and conclusions, or recommendations expressed in this publication are those of the authors and do not necessarily reflect the views of the National Science Foundation.

REFERENCES

Acevedo, O. C., and D. R. Fitzjarrald, 2003: In the core of the night—Effects of intermittent mixing on a horizontally heterogeneous surfaces. *Bound.-Layer Meteor.,* **106,** 1–33.

Balsley, B., D. Fritts, R. Frehlich, R. M. Jones, S. Vadas, and R. Coulter, 2002: Up-gully flow in the great plains region: A mechanism for perturbing the nighttime lower atmosphere? *Geophys. Res. Lett.,* **29,** 1931, doi:10.1029/2002GL015435.

——, R. G. Frehlich, M. L. Jensen, Y. Meillier, and A. Muschinski, 2003: Extreme gradients in the nocturnal boundary layer: Structure, evolution, and potential causes. *J. Atmos. Sci.,* **60,** 2496–2508.

Banta, R. M., 2008: Stable-boundary-layer regimes from the perspective of the low-level jet. *Acta Geophys.,* **56,** 58–87.

——, R. K. Newsom, J. K. Lundquist, Y. L. Pichugina, R. L. Coulter, and L. Mahrt, 2002: Nocturnal low-level jet characteristics over Kansas during CASES-99. *Bound.-Layer Meteor.,* **105,** 221–252.

——, Y. L. Pichugina, and R. K. Newsom, 2003: Relationship between low-level jet properties and turbulence kinetic energy in the nocturnal stable boundary layer. *J. Atmos. Sci.,* **60,** 2549–2555.

——, ——, and W. A. Brewer, 2006: Turbulent velocity-variance profiles in the stably boundary layer generated by a nocturnal low-level jet. *Quart. J. Roy. Meteor. Soc.,* **63,** 2700–2719.

——, L. Mahrt, D. Vickers, J. Sun, B. B. Balsley, Y. L. Pichugina, and E. J. Williams, 2007: The very stable boundary layer on nights with weak low-level jets. *J. Atmos. Sci.,* **64,** 3068–3091.

Blumen, W., R. Banta, S. P. Burns, D. C. Fritts, R. Newsom, G. S. Poulos, and J. Sun, 2001: Turbulence statistics of a Kelvin-Helmholtz billow event observed in the night-time boundary layer during the Cooperative Atmosphere-Surface Exchange Study field program. *Dyn. Atmos. Oceans,* **34,** 189–204.

Burns, S. P., and J. Sun, 2000: Thermocouple temperature measurements from the CASES-99 main tower. Preprints, *14th Symp. on Boundary Layer and Turbulence,* Snowmass, CO, Amer. Meteor. Soc., 358–361.

Canuto, V. M., 2002: Critical Richardson numbers and gravity waves. *Astron. Astrophys.,* **384,** 1119–1123.

Darby, L. S., and Coauthors, 2002: Vertical variations in O_3 concentrations before and after a gust front passage. *J. Geophys. Res.,* **107,** 4176, doi:10.1029/2001JD000996.

Doran, J. C., 2004: Characteristics of intermittent turbulent temperature fluxes in stable conditions. *Bound.-Layer Meteor.,* **112,** 241–255.

Drue, C., and G. Heinemann, 2007: Characteristics of intermittent turbulence in the upper stable boundary layer over Greenland. *Bound.-Layer Meteor.,* **124,** 361–381.

Einaudi, F., and J. J. Finnigan, 1993: Wave-turbulence dynamics in the stably stratified boundary layer. *J. Atmos. Sci.,* **50,** 1841–1864.

Fritts, D. C., C. Nappo, D. M. Riggin, B. B. Balsley, W. E. Eichinger, and R. K. Newsom, 2003: Analysis of ducted motions in the stable nocturnal boundary layer during CASES-99. *J. Atmos. Sci.,* **60,** 2450–2472.

Galperin, B., S. Sukoriansky, and P. S. Anderson, 2007: On the critical Richardson number in stably stratified turbulence. *Atmos. Sci. Lett.,* **8,** 65–69, doi:10.1002/asl.153.

Glickman, T. S., 2000: *Glossary of Meteorology*. 2nd ed. American Meteorological Society, 855 pp.

Grachev, A. A., C. W. Fairall, P. Ola, G. Persson, E. L Andreas, and P. S. Guest, 2005: Stable boundary-layer scaling regimes: The Sheba data. *Bound.-Layer Meteor.,* **116,** 201–235.

Grund, C. J., R. M. Banta, J. L. George, J. N. Howell, M. J. Post, R. A. Richter, and A. M. Weickmann, 2001: High-resolution Doppler lidar for boundary-layer and cloud research. *J. Atmos. Oceanic Technol.,* **18,** 376–393.

Holtslag, A. A. M., and H. A. R. De Bruin, 1988: Applied modeling of nighttime surface energy balance over land. *J. Appl. Meteor.,* **27,** 689–704.

Howell, J. F., and J. Sun, 1999: Surface-layer fluxes in stable conditions. *Bound.-Layer Meteor.,* **90,** 495–520.

Mahrt, L., 1999: Stratified atmospheric boundary layers. *Bound.-Layer Meteor.,* **90,** 375–396.

——, 2008: Bulk formulation of surface fluxes extended to weak-wind stable conditions. *Quart. J. Roy. Meteor. Soc.,* **134,** 1–10.

——, 2010a: Computing turbulent fluxes near the surface: Needed improvements. *Agric. For. Meteor.,* **150,** 501–509.

——, 2010b: Variability and maintenance of turbulence in the very stable boundary layer. *Bound.-Layer Meteor.,* **135,** 1–18.

——, and D. Vickers, 2006: Extremely weak mixing in stable conditions. *Bound.-Layer Meteor.,* **119,** 19–39.

——, J. Sun, W. Blumen, T. Delany, and S. Oncley, 1998: Nocturnal boundary-layer regimes. *Bound.-Layer Meteor.,* **88,** 255–278.

McNider, R. T., D. E. England, M. J. Friedman, and X. Shi, 1995: Predictability of the stable atmospheric boundary layer. *J. Atmos. Sci.,* **52,** 1602–1614.

Meillier, Y. P., R. G. Frehlich, R. M. Jones, and B. B. Balsley, 2008: Modulation of small-scale turbulence by ducted gravity waves in the nocturnal boundary layer. *J. Atmos. Sci.,* **65,** 1414–1427.

Newsom, R. K., and R. M. Banta, 2003: Shear-flow instability in the stable nocturnal boundary layer as observed by Doppler lidar during CASES-99. *J. Atmos. Sci.,* **60,** 16–33.

Panofsky, H. A., and R. A. McCormick, 1960: The spectrum of vertical velocity near the surface. *Quart. J. Roy. Meteor. Soc.,* **86,** 495–503.

Pichugina, Y. L., R. M. Banta, N. D. Kelley, B. J. Jonkman, S. C. Tucker, R. K. Newsom, and W. A. Brewer, 2008: Horizontal-velocity and variance measurements in the stable boundary layer using Doppler lidar: Sensitivity to averaging procedures. *J. Atmos. Oceanic Technol.,* **25,** 1307–1327.

Poulos, G. S., and Coauthors, 2002: CASES-99—A comprehensive investigation of the stable nocturnal boundary layer. *Bull. Amer. Meteor. Soc.,* **83,** 555–581.

Sun, J., 2011: Vertical variations of mixing lengths under neutral and stable conditions during CASES-99. *J. Appl. Meteor. Climatol.,* **50,** 2030–2041.

——, and Coauthors, 2002: Intermittent turbulence associated with a density current passage in the stable boundary layer. *Bound.-Layer Meteor.,* **105,** 199–219.

——, and Coauthors, 2004: Atmospheric disturbances that generate intermittent turbulence in nocturnal boundary layers. *Bound.-Layer Meteor.,* **110,** 255–279.

Van de Wiel, B. J. H., A. F. Moene, O. K. Hartogensis, H. A. R. D. Bruin, and A. A. M. Holtslag, 2003: Intermittent turbulence in the stable boundary layer over land. Part III: A classification for observations during CASES-99. *J. Atmos. Sci.,* **60,** 2509–2522.

Vickers, D., and L. Mahrt, 2003: The cospectral gap and turbulent flux calculations. *J. Atmos. Oceanic Technol.,* **20,** 660–672.

——, and ——, 2006: A solution for flux contamination by mesoscale motions with very weak turbulence. *Bound.-Layer Meteor.,* **118,** 431–447.

Zilitinkevich, S. S., T. Elperin, N. Kleeorin, and I. Rogachevskii, 2007: Energy- and flux-budget (EFB) turbulence closure model for stably stratified flows. Part I: Steady-state, homogeneous regimes. *Bound.-Layer Meteor.,* **125,** 167–191.